HHS Public Access

Author manuscript

J Inherit Metab Dis. Author manuscript; available in PMC 2023 May 01.

Published in final edited form as:

J Inherit Metab Dis. 2022 May ; 45(3): 529–540. doi:10.1002/jimd.12492.

Characterization of exonic variants of uncertain significance in very long-chain acyl-CoA dehydrogenase identified through newborn screening

Olivia M. D'Annibale[1,2], **Erik A. Koppes**[1], **Meena Sethuraman**[3], **Kaitlyn Bloom**[1], **Al-Walid Mohsen**[1,2], **Jerry Vockley**[1,2,*]

[1]Division of Genetic and Genomic Medicine, Department of Pediatrics, University of Pittsburgh School of Medicine, and UPMC Children's Hospital of Pittsburgh, Pittsburgh, PA 15224;

[2]Department of Human Genetics, University of Pittsburgh Graduate School of Public Health, Pittsburgh, PA 15261;

[3]University of Pittsburgh School of Medicine, Pittsburgh, PA 15261.

Abstract

Very long-chain acyl-CoA dehydrogenase deficiency (VLCADD) is an autosomal recessive disease resulting from mutations in the *ACADVL* gene and is among the disorders tested for in newborn screening (NBS). Confirmatory sequencing following suspected VLCADD NBS results often identifies variants of uncertain significance (VUS) in the *ACADVL* gene, leading to uncertainty of diagnosis and providing effective treatment regimen. Currently, *ACADVL* has >300 VUSs in the ClinVar database that requiring characterization to determine potential pathogenicity. In this study, CRISPR/Cas9 genome editing was used to knock out *ACADVL* in HEK293T cells, and targeted deletion was confirmed by droplet digital PCR. No VLCAD protein was detected and an 84% decrease in enzyme activity using the ETF fluorescence reduction assay and C21-CoA as substrate was observed compared to control. Plasmids containing control or variant *ACADVL* coding sequence were transfected into the *ACADVL* null HEK293T. While transfection of control *ACADVL* restored VLCAD protein and enzyme activity, cells expressing the VLCAD Val283Ala mutant had 18% VLCAD enzyme activity and reduced protein compared to control. VLCAD

*Correspondence: Jerry Vockley, vockleyg@upmc.edu, 4401 Penn Avenue Pittsburgh, PA 15224.

Author Contributions

OMD reviewed literature, completed most experiments, statistical anlaysis, and drafted the manuscript. EAK developed experimental design, manuscript preparation, and reviewed manuscript. Meena Sethuraman compiled patient data and performed some laboratory experiments. KB assisted with some laboratory experiments. A-WM conducted enzyme modeling, manuscript preparation, and reviewed manuscript. JV developed the experimental design. All authors discussed the results and contributed to the final manuscript.

Conflict of Interest

All authors certify that they have no affiliations with or involvement in any organization or entity with any financial or non-financial interest in the subject matter or materials discussed in this manuscript.

Compliance with Ethics Guidelines

Informed Consent

This article does not contain any studies with human subjects performed by any of the authors. To obtain fibroblast cell samples, informed consent forms were signed by patients or patients' legal guardians for use in research. In addition, patients' names were anonymized.

Animal Rights

This article does not contain any studies with animal subjects performed by any of the authors.

There are no other data associated with this manuscript other than is included in the manuscript.

Ile420Leu, Gly179Arg, and Gln406Pro produced protein comparable to control but 25%, 4%, and 5% VLCAD enzyme activity, respectively. Leu540Pro and Asp570_Ala572dup had reduced VLCAD protein and 10% and 3% VLCAD enzyme activity, respectively. VLCADD fibroblasts containing the same variations had decreased VLCAD protein and activity comparable to the transfection experiments. Generating *ACADVL* null HEK293T cell line allowed functional studies to determine pathogenicity of *ACADVL* exonic variants. This approach can be applied to multiple genes for other disorders identified through NBS.

Keywords

Very-long chain acyl-CoA dehydrogenase (VLCAD) deficiency; inborn errors of metabolism; newborn screening; variants of uncertain significance; fatty acid oxidation disorders; high throughput screening

Introduction

Very long-chain acyl-CoA dehydrogenase (VLCAD) deficiency (OMIM 201475) is an autosomal recessive disorder caused by biallelic mutations in the *ACADVL* gene, 17p13.1 [1]. VLCAD catalyzes the first intra-mitochondrial step of the mitochondrial β-oxidation of long-chain fatty acids with carbon length chain of 14 to 20 [1, 2]. The frequency of VLCADD is about 1:30,000 to 1:100,000 live births world [3, 4]. Symptoms of VLCADD include hypoglycemia, recurrent rhabdomyolysis, myopathy, hepatopathy, and cardiomyopathy and can present in infancy or later in childhood or adulthood [5]. Treatment for VLCADD patients involves a reduced-fat diet containing medium chain triglyceride (MCT) or triheptanoin supplementation and avoidance of high stress and exercise [6–9]. In the United States and many other developed countries, VLCAD deficient patients are identified through newborn screening of dried spots with an elevated C14:1 and/or C14:1/C12:1 ratio [3]. Ultimate outcome is improved by identification of the disorder through newborn screening [10–12]. However, many patients upon follow up sequencing of *ACADVL* are found to have at least one VUS. As of this writing, there are over 350 VUSs in the ClinVar database.

Quantitating characteristic metabolites from dried blood spots by tandem mass spectrometry (MS/MS) is the clinical standard of care for newborn screening (NBS) for many inborn errors of metabolism, but requires genetic or functional follow up testing to confirm a diagnosis [13]. Increasingly diagnosis by molecular analysis through targeted, exome or whole-genome DNA sequencing is becoming the *de facto* norm for many disorders. Given the only recent emergence of these technologies as employed to diagnose rare-diseases there are only a limited number of clinically described and annotated pathogenic alleles. Therefore, DNA sequencing-based diagnostic methods often result in identification of variants of uncertain significance (VUS) in at least one allele, leading to uncertainty of the diagnosis [14]. In this situation, a definitive diagnosis can only be made through functional testing (*e.g.* enzymatic activity assays from patient dermal fibroblast), which is often either not available or cumbersome to obtain and can lead to a significant delay of treatment implementation [14, 15].

In this study, we describe a scalable approach to determine the functional significance of VUSs identified by NBS in a timely manner to facilitate better diagnostic and therapeutic outcomes. We have previously developed an *IVD* null HEK293T model to screen VUS mutations in *IVD* [16]. Here we present an expansion of this system by examining the functional effect of VUSs identified in newborns in an *ACADVL* null HEK293T cell line generated with CRISPR/Cas9 genome-editing. This model enables determination of pathogenicity of individual *ACADVL* VUSs, and is amendable for development as a high through put platforms for screening VUSs in other inborn errors of metabolism.

Materials and Methods

Experiments were performed in accordance with the approved guidelines and regulations. Experimental human protocols were approved by the Institutional Review Board at the University of Pittsburgh, protocol 19030195.

Subjects

Subjects were identified through abnormal NBS with elevation of C14:1-carnitine consistent with VLCAD deficiency (Supplementary Table 1). Sequencing of *ACADVL* was performed on a clinical basis in a CLIA certified laboratory on the proband and parents to determine *ACADVL* mutation and phase. Amino acid variants are presented relative to the precursor form fo the enzyme. Skin biopsies for fibroblast culture were performed on a clinical basis from infants with consent of parents and/or legal guardians. Control fibroblast cells were obtained from the American Type Culture Collection (ATCC.org).

Cell lines & culture

HEK293T (obtained from the American Type Culture Collection) and fibroblast cell lines were grown in Dulbecco's Modified Eagle Medium (DMEM; Corning Life Sciences, Manassas, VA) containing 4.5 g/L glucose and supplemented with 10% fetal bovine serum, 4 mM glutamine and 100 IU penicillin and 100 μg/ml streptomycin (Corning Life Sciences, Manassas, VA) at 37 °C in a 5% CO_2 humidified atmosphere.

CRISPR/Cas9 genome-editing

Genome-editing of HEK293T cells using a plasmid vector based CRISPR/Cas9 strategy was accomplished as described before [16]. In brief, we utilized single-guide RNAs (sgRNAs) within *ACADVL* exon 12 and exon 16 cloned into pSpCas9(BB)-2A-GFP vector (PX458; Addgene #48138) [17] to generate deletions of the intervening *ACADVL* sequence encoding a crucial region of the catalytic domain. Following plasmid transfection and single-cell GFP(+) flow sorting clonal genome-edited lines were scaled up and screened by breakpoint deletion PCR and positive clones further analyzed by *ACADVL* copy number and VLCAD protein assays. Oligonucleotides used for sgRNA cloning adapters and breakpoint deletion PCR primers are listed in Supplementary Table 2.

Western blot

Fibroblasts and HEK293T cells were grown in T175 flasks to 90% confluence, harvested by trypsinization, pelleted, and stored at −80°C for western blot. Frozen pellets were treated

with 50 μL of radioimmunoprecipitation assay (RIPA) buffer (Thermofisher Scientific) and 1X Protease Inhibitor Cocktail (PI) (Roche, St Louis, MO) for 30 minutes on ice and centrifuged at 14,000 x g for 15 minutes at 4°C. Supernatants were collected and 25 μg of protein was loaded onto a 4 to 15% gradient Criterion precast SDS-PAGE gel (Biorad, Hercules, CA). Following electrophoresis, the gel was blotted onto a nitrocellulose membrane and incubated with mouse anti-ACADVL antibody (1:2000; Invitrogen, Waltham, MA), then incubated with secondary goat anti-mouse-HRP antibody (1:3000, Biorad). Pierce ECL Western Blotting Substrate kit (Thermofisher Scientific) was used to visualize bands. Membranes were stripped and re-probed with mouse anti-glyceraldehyde 3-phosphate dehydrogenase (GAPDH; 1:25,000) monoclonal antibody (Abcam, Cambridge, MA) to verify equal loading.

ETF fluorescence reduction assay via cuvette

The electron transfer flavoprotein (ETF) fluorescence reduction assay was performed using a Jasco FP-6300 spectrofluorometer (Easton, MD) with cuvette holder heated with circulating water at 32°C, as previously described [18, 19]. ETF was diluted 1200-fold into a buffer containing 50 mM Tris, pH 8.0, 5 mM EDTA and 50% glycerol, and 10 μl were used for each assay. The ETF concentration in the reaction mixture was 2 μM. 30 μM of palmitoyl-CoA lithium salt hydrate (C16-CoA; Sigma-Aldrich Co., St. Louis, MO) or heneicosanoyl-CoA ammonium salt (C21-CoA; Avanti Polar Lipids, Alabaster, AL) were used to measure VLCAD activity. 30 μM of octanoyl-CoA lithium salt hydrate (C8-CoA; Sigma Aldrich Co.) was used to measure medium chain acyl-CoA dehydrogenase (MCAD) activity. Spectra Manager 2 software (Jasco, Inc.) was used to collect data and calculate reaction rate and Microsoft Excel was used to calculate kinetic parameters.

ETF fluorescence reduction assay via microplate

Recombinant pig ETF was purified according to the method published earlier [20]. A microtiter plate adaptation of the ETF fluorescence reduction assay was performed using FLUOstar Omega (BMG Labtech, Cary, NC) microplate reader set to 32°C, with excitation/emission wavelengths of Ex_{340}/Em_{490} as previously described [18–20]. Briefly, the final reaction volume of 200 μl contain 30 μg of sample and the ETF concentration, glucose/oxidase concentrations and substrate concentration were the same as for the cuvette assay. Sample and all reagents except substrate were added in triplicate to a glass-bottomed, black walled plate. With background fluorescence zeroed. Baseline ETF fluorescence was monitored for 60 s, substrate was added with a multi-channel pipettor, and the plate was immediately read for another 60 s. Slopes and Y-intercepts were automatically calculated by the instrument software and enzymatic activity was calculated in Microsoft Excel.

Digital droplet polymerase chain reaction (ddPCR)

Copy number assays using ddPCR probe-based assays were designed and completed as previously described [16]. Genomic DNA from parental HEK293T and *ACADVL* CRISPR-Cas9 targeted clonal lines, was restriction digested with *EcoRI*-HF (New England Biolabs, Ipswich, MA) and diluted to a concentration of 20 ng/μl with 2 μl used as input per reaction. Multiplex ddPCR assays utilized PrimeTime 5′ nuclease probes (IDT, Coralville, IA) which were FAM labeled for *ACADVL* intron 11 and exons 10, 15, or 20 and HEX

labeled for the autosomal *RPP30* reference locus (Oligonucleotide probe and primers given in Supplemental Table 3). The ddPCR reactions were run on an automated droplet generator and QX200 reader (Biorad). The genomic copy number of the target *ACADVL* region was calculated under the assumption that *RPP30* was diploid (i.e. the ratio of the concentration of target *ACADVL* amplicon to *RPP30* multiplied by 2) with a 95% confidence interval indicated by Poisson statistics [21].

ACADVL variant vector design and isolation

Control and variant *ACADVL* gene pcDNA3.1(+) mammalian expression vectors were constructed by BioMatik (Willmington, DE). To produce the expression plasmids in amounts for transfection experiments, *ACADVL* pcDNA3.1(+) vectors were transformed into XL-1-Blue supercompetent Escherichia coli (Agilent Technologies, Santa Clara, CA) and grown in Luria-Bertani (LB) broth and 100 μg/mL ampicillin. Plasmids DNA were isolated using a midi prep kit (Zymo Research, Irvine, CA).

Transfection of ACADVL mutant vectors

ACADVL null HEK293T cells were seeded into 6-well plates or 10 cm^2 dishes and co-transfected with 2.5 or 15 μg of plasmid DNA, respectively, at 60% confluency using *Trans*IT X2 (Mirus Bio LLC, Madison, WI). Cells were incubated for 48 hours and then harvested for western blotting and ETF reduction assay for VLCAD protein presence and enzyme activity.

ACADVL cDNA analysis

ACADVL variant plasmid transfected *ACADVL* null HEK293T mRNA was isolated using an RNeasy Mini kit with on column DNaseI digestion (Qiagen). First strand synthesis of complementary DNA (cDNA) from 500 ng of mRNA was performed using the Superscript Vilo IV Master Mix (Qiagen). Reverse transcription PCR (RT-PCR) of full-length and partial *ACADVL* cDNA regions was performed with Q5 DNA polymerase (New England Biolabs). Quantitative PCR was performed with equivalent amount of cDNA on a Bio-Rad CFX96 Real-Time PCR Instrument, with SYBR Green Master Mix (Thermo Fisher Scientific). *ACADVL*, and *GAPDH* were assayed (Supplementary Table 4). Expression levels were normalized to *GAPDH* and the data were analyzed by the $2^{-\Delta\Delta Ct}$ method [22].

ACADVL mutant modeling

VLCAD structure visualization and mutation modeling was performed using a Silicon Graphics Fuel workstation (Mountain View, CA) and the *Insight* II 2005 software package, using the atomic coordinates of recombinant human VLCAD (pdb code: 3B96) [23]. Residues at the mutation sites were replaced manually and best energy conforming conformation, with least energy fit, was adopted for further analysis of interactions with juxtaposed residues.

Results

CRISPR/Cas9 ACADVL gene editing

To generate a cell culture model in which to study *ACADVL* mutations with unknown functional significance we employed CRISPR-Cas9 genome-editing to introduce null mutations into the HEK293T cell line. A dual sgRNA strategy was used to induce double-stranded DNA breaks at *ACADVL* exons 12 to 16 and delete the intervening region (Figure 1A), including exon 15 encoding key residues of the VLCAD catalytic core [23]. From 24 clonally isolated HEK293T CRISPR-Cas9 transfected cells mutations were detected by deletion breakpoint-PCR in 14 clonal lines(Supplemental Figure 1A–C). Further characterization of candidate genome-edited clonal lines by genomic copy number ddPCR identified 4 clonal lines (A1–02, A1–07, A1–11 and A1–15) without an intact copy of *ACADVL* exon 15 (Figure 1B, Supplemental Figure 1D). Not unexpectedly, given the heterogenous chromosomal ploidy in HEK293T [24, 25], and our previous genome editing study deriving *IVD* null HEK293T lines [16], normalization of *ACADVL* ddPCR amplicons to *RPP30* yielded evidence for an *ACADVL* haploid line with a deletion (A1–02), one diploid line with homozygous ACADVL deletion (A1–11), and two *ACADVL* diploid lines in with both copies harbored a deletion but which were triploid for RPP30 (A1–07 and A1–15) (Figure 1B).

Functional characterization of ACADVL null HEK293T cells

Each of the four genome-edited clonal lines with deleted *ACADVL* exon 15 (A1–02, A1–07, A1–11 and A1–15; Figure 1) were shown to lack detectable expression of the VLCAD protein by western blotting, thereby confirming the null mutations (Figure 2A). VLCAD and MCAD activity were assessed using the ETF fluorescence reduction assay (Fig. 2B,C). All *ACADVL* null HEK293T clones had reduced enzyme activity measured with C16-CoA as substrate (Fig. 2B: 36 to 41% of control HEK293T). As expected, there was no statistical difference in MCAD activity between the control and clones (Fig. 2C). The remaining activity detected by palmitoyl-CoA is related to long-chain acyl-CoA dehydrogenase (LCAD) and acyl-CoA dehydrogenase family member 9 (ACAD9) activity. To determine the level of LCAD activity, we used 2,6-dimethylheptanoyl-CoA, a specific substrate of LCAD [26]. LCAD activity was not statistically different in control and A1–7 clone (Fig. 3D).To diminish the contribution of the other ACADs having long chain activity on measuring VLCAD activity using the ETF fluorescence reduction assay, we next measured the ACAD activity using heneicosanoyl-CoA (C21-CoA), which is best utilized by VLCAD compared to LCAD and ACAD9 [27]. Clone A1–7 had reduced activity using both 16-CoA and C21-CoA compared to control, but the apparent reduction was greater with the more specific substrate, 42% and 16%, respectively, (Fig. 3A,B). While MCAD was reduced in clone A1–7 compared to control, it is still within a range seen in other experiments (Fig. 3C).

Based on the absence of VLCAD protein and activity, we selected clone A1–7 as our *ACADVL* null HEK293T cell line and used this cell line for all additional experiments, and performed subsequent long chain assays with C21-CoA.

Genetic and functional validation of variants of uncertain significance in VLCAD deficient fibroblasts

Fibroblasts from five VLCADD patients based on metabolite parameters and clinically determined variants, including at least one VUS, were analyzed for VLCAD activity using the cuvette based ETF fluorescence reduction assay (Supplementary Table 1). All five cell lines had reduced VLCAD protein presence in cell lysates as determined by western blotting (Fig. 4A) and reduced VLCAD enzyme activity compared to control (Fig. 4B), consistent with clinically defined diagnosis. LCAD activity was not measured as fibroblasts have previously been shown to contain no LCAD enzyme [28]. All five VLCADD cell lines had variable changes in MCAD activity compared to a concurrent control, but within the normal variation seen in fibroblasts (Fig. 4C).

Functional analysis of individual VUS alleles in HEK293T ACADVL null lines

To evaluate the effect of *ACADVL* VUS alleles, we evaluated VLCAD protein and enzymatic activity in *ACADVL* null HEK293T cells that were transfected with vectors driving expression of normal consensus *ACADVL* cDNA or *ACADVL* cDNA containing individual mutations from variants identified in the VLCAD deficient patients (Table 1, Fig. 5). RT-PCR and qPCR analysis confirmed there was no *ACADVL* expression in the HEK293T knock out cells, and that all transfected cells had abundant levels of *ACADVL* mRNA, confirming that the expression plasmid was expressing the *ACADVL* gene properly (Fig. 5A). Abundant VLCAD protein levels were observed with transfection of control, c.848T>C (p.Val283Ala), c.1248A>C (p.Ile420Leu), c.535G>A (p.Gly179Arg), and c.1217A>C (p.Gln406Pro) inserts (Fig. 5B). In contract, VLCAD protein was barely observed following expression with c.1619T>C p.(Leu540Pro) and c.1707_1715dup (p.Asp570_Ala572dup) inserts (Fig. 5B). Expression of the control cDNA in *ACADVL* null HEK293T cells led to dramatic increase in VLCAD activity (Fig. 5C and D). All tested variants showed little or no enzyme activity using either C16- or C21-CoA as substrate (Fig. 5C and D). Extracts from cells expressing the common variant, c.848T>C (p.Val283Ala) had 18% of the control plasmid activity as measured with C21-CoA, consistent with previous reports of 22% VLCAD activity compared to control in fibroblasts [29, 30]. MCAD activity varied in cells expressing the variant *ACADVL* cDNAs, though still well above the VLCAD levels (Fig. 5E).

Computational prediction of mutation's adverse structure/function effect

The effect of the mutations reported in this study can be further evaluated using *in silico* molecular modeling that can bring structure function relationship insights. Val283Ala and Ile420Leu are predicted to be the most stable among the mutations. The latter is the most intriguing of the two since despite being a conservative replacement there is an obvious detectable adverse effect on enzyme activity and stability. Ile420 is located at the interface between the ACAD-like catalytic domain and the C-terminus region that replaces the third, or fourth, monomer region in the tetrameric version (Fig. 6). The C-terminus domain is believed to function to anchor the protein to the long chain fatty acid β-oxidation complex, membrane, or other macromolecule. The Ile420 residue is part of a hydrophobic pocket that provide stability to the ACAD-like domain C-terminus domain interface (Fig. 6). It

is located near the middle of α-Helix I and is at interacting distance on one side with Leu468 and Val472, further distance from Ala416 and Ile417, and across from Ile573 of the C-terminus α-helix M (Fig. 6). Key to Ile420 residue's importance seems to be its apparent dual role as part of this hydrophobic pocket. It has a particularly important anchoring interaction to the C-terminus with Ile573, but it also enhances the tightness of the salt bridge formed between Arg469 and Glu424. The salt bridge between these two residues is conserved in ACAD9, the homologous dimeric ACAD. The ε-N of the Arg469 guanidinium group is in close interacting proximity with the carboxylate of Asp570 of the C-terminus α-helix M. Replacement of Ile420 with a Leu, albeit slightly tolerated, partially disrupts the intricate proximity to the salt bridge (Fig. 6). While in ACAD9 the equivalent residue to Ile420 is a Val, the orientation of the Val side chain can likely interact better with the equivalent salt bridge.

Gln406 is located at the N-terminus of the loop connecting α-helices H and I. A change to proline at any position is usually assumed to be devastating for protein structure unless, it is in a loop and the trajectory or the secondary and tertiary fold of structurally important peptide to the C-terminus side is not affected. In this case, VLCAD Gln406Pro was detectable in appreciable amounts in the HEK293T cells expressing the mutant. This implies that despite this being a folding mutation, some protein might yet be present in cells and that will be amenable to chaperone therapy.

The mutations Asp570_Ala572dup and Leu540Pro are in the middle of α-helices M and N, respectively, of the C-terminus and are expected to be detrimental to structural stability. Gly179 is located at the active site as part of α-helix E. While its replacement with an Arg would affect folding, it seems to be energetically well tolerated as the side chain sits in the active site. However, the positioning would prevent substrate binding.

Discussion

We have previously confirmed pathogenicity of *ACADVL* mutations directly in patient fibroblasts using a prokaryotic system and a relatively large volume cuvette assay as well as a high throughput microtiter plate assay [29, 31]. However, establishing a fibroblast culture requires and invasive procedure in a newborn as well as significant time to grow to sufficient quantity to be assayed. In theory, direct measurement of enzyme activity in patient white blood cells is possible, the assay is also not available clinically in many jurisdictions. In addition, most VLCAD deficient patients have unique combinations of variants and the relative effect of each cannot be addressed with either fibroblast or white blood cell assays, nor does either allow testing pathogenicity of VUSs in genetic dfatabases. We have recently developed *IVD* and *ACAD9* null HEK293T lines to assess *IVD* and *ACAD9* variant pathogenicity, respectively [16, 32]. In this study, we describe the generation of a deletion in the *ACADVL* gene in HEK293T cells using CRISPR/Cas9 technology that can similarly be used to study expression of variant recombinant proteins [33]. To better address the need for rapid turnaround time, we utilized a commercial gene synthesis service to rapidly generate *ACADVL* variants for expression in our *ACADVL* null HEK293T cells, and then confirmed that our microtiter plate assay gave a robust differentiation between control and inactivating variant containing inserts. Because this assay requires less sample, the time from

transfection to assay was also minimized compared to fibroblast cultures. Plasmid design and ordering requires 1 day and are typically delivered in 2–4 weeks. Transformation of E. coli with *ACADVL* plasmid colony selection, and midi prep of culture is 4 days. Seeding of ACADVL null HEK293T cells requires 1 day, transfection of ACADVL plasmid 2 day incubation, and harvest of plates requires 1 day. Traditional western blotting requires 2 days for results and the ETF fluorescent reduction microplate assay requires 3 hours to measure all 7 plasmids described in this manuscript in triplicates of 3 Co-A substrates compared to 2–3 days to measure the same amount of samples in the traditional cuvette assay. Thus, from the time of receiving the variant plasmid until final result was 11 days.

To test this system, we examined the pathogenicity of 5 variants previously designate VUSs in the ClinVar database, as well as the effect on activity of the common *ACADVL* variant identified through NBS. RNA expression levels of the plasmid were similar across all mutations, supporting that changes in protein levels or enzyme activity were due to the mutation introduced into the *ACADVL* insert. The inactivating nature of each of the variants agreed with the more laborious and time-consuming fibroblast assays from the patients in which each variant was detected originally. In this regard, our approach can be used to address the pathogenicity of VUSs in any gene in which a clear biochemical marker can be measured following transfection of an expression plasmid into easily made HEK293T (or other) cells. Thus, our plate ACAD assay can easily measure the activity of any of the other ACAD deficiencies identified by newborn screening (IVD, IBD, SBCAD, and MCAD). Similarly, any defects identified by tandem mass spectrometry could easily measure accumulation of the diagnostic metabolite in the cellular medium as an indicator of pathogenicity. While in theory, measurement of long chain acylcarnitines in the mediua of cultured cells is also possible, the knock out HEK293T cells did not accumulate high enough baseline levels to allow quantification of reduction to be a viable assay. Of note, only one VUS in *ACADVL* was identified by clinical sequencing in three patients in this study even though they clearly had VLCAD deficiency based on clinical presentation and fibroblast testing. While we were able to confirm the pathogenicity of the VUS identified in each patient, we did not undertake additional experiments to identify the second mutation in these cell lines. It is interesting that while C21-CoA is less efficiently used as substrate for control VLCAD (Fig. 3), the effect is not consistent in the mutant enzymes (Fig. 5) This presumable is due to structural variations induced by each mutation that lead to changes in the substrate binding pocket. However, we did not further explore this possibility.

Based on this study, we propose that the VUSs examined be reclassified in ClinVar. Variants c.1619T>C, (p.Leu540Pro), c.1707_1715dup, (p.Asp570_Ala572dup), c.1248A>C, (p.Ile420Leu), c.535G>A (p.Gly179Arg), and c.1217A>C, (p.Gln406Pro) be reclassified from VUS to pathogenic/likely pathogenic; and c.848T>C, (p.Val283Ala) should maintain its pathogenic status.

In this study we were able to apply the high throughput ETF fluorescence reduction microplate assay over the traditional cuvette assay. The application of the microplate version of the assay allowed us to decrease reagent amount and time required for the assay [20]. This allowed us to screen more variants, in a shorter time frame. This microplate assay can be applied to any of the acyl-CoA dehydrogenases. Application of acylcarnitine

profiling through tandem mass spectrometry in media collected from cultured cells to allow for confirmation of pathogenicity for disorders without an enzyme activity assay. The addition specifically of the ETF fluorescence reduction microplate assay will allow for rapid confirmation of *ACADVL* variant pathogenicity in infants identified through NBS without the need for an invasive procedure such as a skin biopsy.

Examining possible adverse effects on structure and function of amino acid residues replacements *in silico* complements these functional studies and leads to important insight into the scope and severity of each defect at the molecular level, potentially suggesting alternative treatment options. For example, concurrent experimental and *in silico* indications of mild structural effect would suggest modification of dietary plans, including dietary recommendations for fat intake. This study also demonstrates that the severity of the effect of mutations in the C-terminus region on protein instability is hard to assess solely from assay of patient cells. For *in silico* modeling provided the impetus to evaluate the effects Ile420Leu in our expression system because of predicted structural plasticity, and the possibility that the mutation could still support production of functional protein. Indeed, while assay of patient cells with this mutation failed to detect VLCAD protein, our expression system instead demonstrated that mutant protein could be stable and thus a candidate for therapy with a molecular chaperonin.

In summary, we have developed an *ACADVL* null HEK293T cell line with no VLCAD protein or activity that allowed determination of pathogenicity of several previous VUSs found in patients with suspected VLCAD deficiency identified through NBS. This model will allow for high throughput assessment of the function of VUSs in multiple genes for disorders identified through NBS, allowing even a saturation mutagenesis approach to assess the impact of all possible mutations in a gene. In addition, our functional expression system in combination with molecular modeling serves as the beginning of a personalized medicine approach that will ultimately allow better targeted therapies for patients.

Supplementary Material

Refer to Web version on PubMed Central for supplementary material.

Acknowledgements

JV was supported in part by NIH grant R01 DK109907. We thank the staff at the Core Flow Cytometry Laboratory from the University of Pittsburgh, UPMC Children's Hospital of Pittsburgh for help with flow sorting of GFP positive cells. We thank Yuxun Zhang, PhD from Eric Goetzman, PhD Laboratory, University of Pittsburgh, Children's Hospital of UPMC for providing ETF for the ETF fluorescence reduction assays.

Funding

This study was funded by JV NIH R01 DK78755.

References

1. Leslie ND, et al., Very Long-Chain Acyl-Coenzyme A Dehydrogenase Deficiency, in GeneReviews((R)), Adam MP, et al., Editors. 1993: Seattle (WA).
2. Wanders RJ, et al. , Disorders of mitochondrial fatty acyl-CoA beta-oxidation. J Inherit Metab Dis, 1999. 22(4): p. 442–87. [PubMed: 10407780]

3. McHugh D, et al. , Clinical validation of cutoff target ranges in newborn screening of metabolic disorders by tandem mass spectrometry: a worldwide collaborative project. Genet Med, 2011. 13(3): p. 230–54. [PubMed: 21325949]
4. American College of Medical Genetics Newborn Screening Expert G, Newborn screening: toward a uniform screening panel and system--executive summary. Pediatrics, 2006. 117(5 Pt 2): p. S296–307. [PubMed: 16735256]
5. Andersen RM, Revisiting the behavioral model and access to medical care: does it matter? J Health Soc Behav, 1995. 36(1): p. 1–10. [PubMed: 7738325]
6. Solis JO and Singh RH, Management of fatty acid oxidation disorders: a survey of current treatment strategies. J Am Diet Assoc, 2002. 102(12): p. 1800–3. [PubMed: 12487544]
7. Behrend AM, et al. , Substrate oxidation and cardiac performance during exercise in disorders of long chain fatty acid oxidation. Mol Genet Metab, 2012. 105(1): p. 110–5. [PubMed: 22030098]
8. Gillingham MB, et al. , Triheptanoin versus trioctanoin for long-chain fatty acid oxidation disorders: a double blinded, randomized controlled trial. J Inherit Metab Dis, 2017. 40(6): p. 831–843. [PubMed: 28871440]
9. Vockley J, et al. , Triheptanoin treatment in patients with pediatric cardiomyopathy associated with long chain-fatty acid oxidation disorders. Mol Genet Metab, 2016. 119(3): p. 223–231. [PubMed: 27590926]
10. Spiekerkoetter U, Mitochondrial fatty acid oxidation disorders: clinical presentation of long-chain fatty acid oxidation defects before and after newborn screening. J Inherit Metab Dis, 2010. 33(5): p. 527–32. [PubMed: 20449660]
11. Hoffmann L, et al. , VLCAD enzyme activity determinations in newborns identified by screening: a valuable tool for risk assessment. J Inherit Metab Dis, 2012. 35(2): p. 269–77. [PubMed: 21932095]
12. Wilcken B, Fatty acid oxidation disorders: outcome and long-term prognosis. J Inherit Metab Dis, 2010. 33(5): p. 501–6. [PubMed: 20049534]
13. Oglesbee D, et al. , Second-tier test for quantification of alloisoleucine and branched-chain amino acids in dried blood spots to improve newborn screening for maple syrup urine disease (MSUD). Clin Chem, 2008. 54(3): p. 542–9. [PubMed: 18178665]
14. Narravula A, et al. , Variants of uncertain significance in newborn screening disorders: implications for large-scale genomic sequencing. Genet Med, 2017. 19(1): p. 77–82. [PubMed: 27308838]
15. Wilcken B, Medicine. Newborn screening: gaps in the evidence. Science, 2013. 342(6155): p. 197–8. [PubMed: 24115426]
16. D'Annibale OM, et al. , Characterization of variants of uncertain significance in isovaleryl-CoA dehydrogenase identified through newborn screening: An approach for faster analysis. Mol Genet Metab, 2021.
17. Ran FA, et al. , Genome engineering using the CRISPR-Cas9 system. Nat Protoc, 2013. 8(11): p. 2281–2308. [PubMed: 24157548]
18. Frerman FE and Goodman SI, Fluorometric assay of acyl-CoA dehydrogenases in normal and mutant human fibroblasts. Biochem Med, 1985. 33(1): p. 38–44. [PubMed: 3994700]
19. Vockley J, et al. , Mammalian branched-chain acyl-CoA dehydrogenases: molecular cloning and characterization of recombinant enzymes. Methods Enzymol, 2000. 324: p. 241–58. [PubMed: 10989435]
20. Zhang Y, et al. , An acyl-CoA dehydrogenase microplate activity assay using recombinant porcine electron transfer flavoprotein. Anal Biochem, 2019. 581: p. 113332. [PubMed: 31194945]
21. Dube S, Qin J, and Ramakrishnan R, Mathematical analysis of copy number variation in a DNA sample using digital PCR on a nanofluidic device. PLoS One, 2008. 3(8): p. e2876. [PubMed: 18682853]
22. Livak KJ and Schmittgen TD, Analysis of relative gene expression data using real-time quantitative PCR and the 2(-Delta Delta C(T)) Method. Methods, 2001. 25(4): p. 402–8. [PubMed: 11846609]
23. McAndrew RP, et al. , Structural basis for substrate fatty acyl chain specificity: crystal structure of human very-long-chain acyl-CoA dehydrogenase. J Biol Chem, 2008. 283(14): p. 9435–43. [PubMed: 18227065]

24. Lin YC, et al. , Genome dynamics of the human embryonic kidney 293 lineage in response to cell biology manipulations. Nat Commun, 2014. 5: p. 4767. [PubMed: 25182477]

25. Bylund L, et al. , Analysis of the cytogenetic stability of the human embryonal kidney cell line 293 by cytogenetic and STR profiling approaches. Cytogenet Genome Res, 2004. 106(1): p. 28–32. [PubMed: 15218237]

26. Wanders RJ, et al. , 2,6-Dimethylheptanoyl-CoA is a specific substrate for long-chain acyl-CoA dehydrogenase (LCAD): evidence for a major role of LCAD in branched-chain fatty acid oxidation. Biochim Biophys Acta, 1998. 1393(1): p. 35–40. [PubMed: 9714723]

27. Izai K, et al. , Novel fatty acid beta-oxidation enzymes in rat liver mitochondria. I. Purification and properties of very-long-chain acyl-coenzyme A dehydrogenase. J Biol Chem, 1992. 267(2): p. 1027–33. [PubMed: 1730632]

28. Chegary M, et al. , Mitochondrial long chain fatty acid beta-oxidation in man and mouse. Biochim Biophys Acta, 2009. 1791(8): p. 806–15. [PubMed: 19465148]

29. Goetzman ES, et al. , Expression and characterization of mutations in human very long-chain acyl-CoA dehydrogenase using a prokaryotic system. Mol Genet Metab, 2007. 91(2): p. 138–47. [PubMed: 17374501]

30. Andresen BS, et al. , Clear correlation of genotype with disease phenotype in very-long-chain acyl-CoA dehydrogenase deficiency. Am J Hum Genet, 1999. 64(2): p. 479–94. [PubMed: 9973285]

31. Schiff M, et al. , Molecular and cellular pathology of very-long-chain acyl-CoA dehydrogenase deficiency. Mol Genet Metab, 2013. 109(1): p. 21–7. [PubMed: 23480858]

32. Schiff M, et al. , Complex I assembly function and fatty acid oxidation enzyme activity of ACAD9 both contribute to disease severity in ACAD9 deficiency. Hum Mol Genet, 2015. 24(11): p. 3238–47. [PubMed: 25721401]

33. Thomas P and Smart TG, HEK293 cell line: a vehicle for the expression of recombinant proteins. J Pharmacol Toxicol Methods, 2005. 51(3): p. 187–200. [PubMed: 15862464]

Synopsis

Generating an *ACADVL* null HEK293T cell line and development of a high-throughput enzymatic expression and assay system facilitates rapid and scalable screening of *ACADVL* variants of uncertain significance identified through newborn screening.

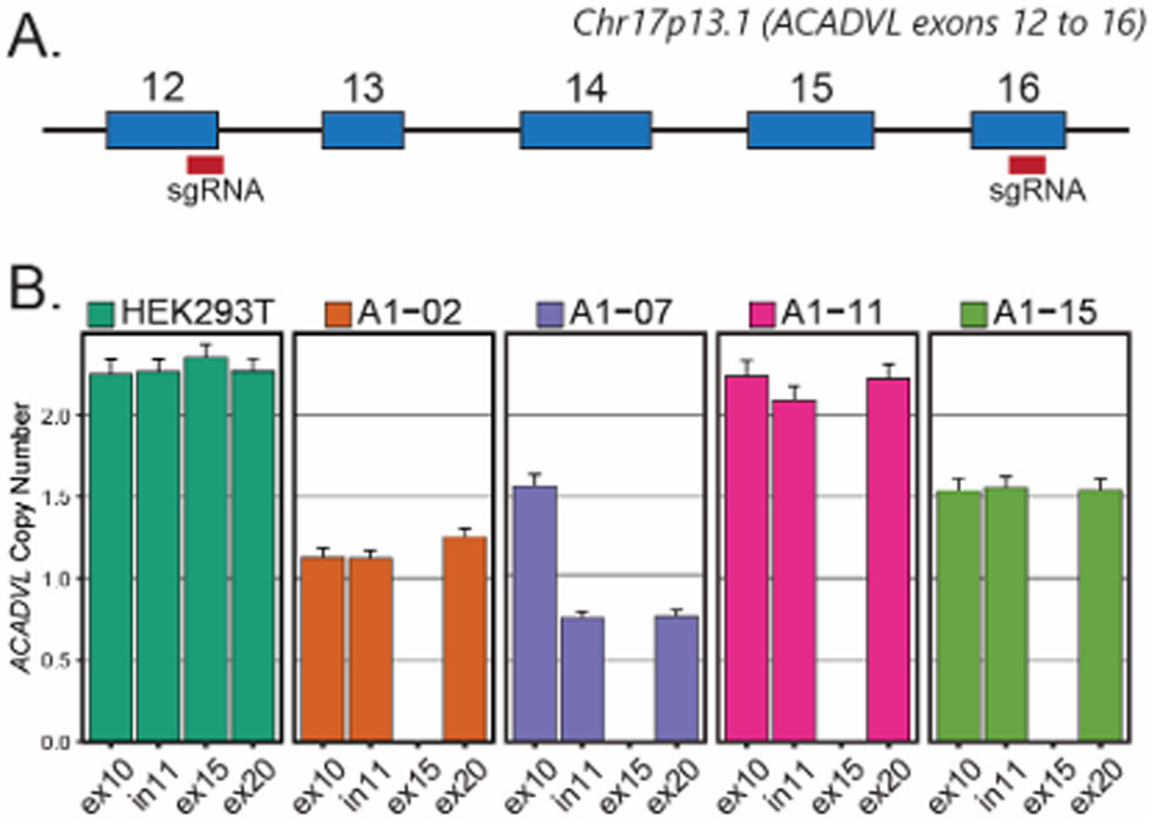

Figure 1: Targeted deletion of *ACADVL* exons 12–16 using CRISPR-Cas9 genome-editing.

(A) Diagram of dual sgRNA CRISPR-Cas9 strategy targeting *ACADVL*. Key: Blue box, *ACADVL* exons with intervening introns; red rectangles, sgRNA sites.. (B) Genomic copy number (CN) of ACADVL exon 10, intron 11, exon 15 and exon 20 as quantified by ddPCR with normalization to the *RPP30* locus. Notably the HEK293T is near diploid (CN=2) for ACADVL across the gene whereas each clonal line exhibited complete loss of the targeted exon 15. A1–02 showed deletion of exon 15 with a haploid number (CN=1) across the untargeted region; A1–07 and A1–15 display deletion of exon15 with an inferred 3N copies of RPP30 leading to CN=1.5 for untargeted regions, with A1–07 likely having one deletion allele extending both into intron 11 proximally and through exon 20 distally; and A1–15 with an expected diploid *ACADVL* deletion pattern with observed CN of 2N at the untargeted regions and 0N at exon 15.

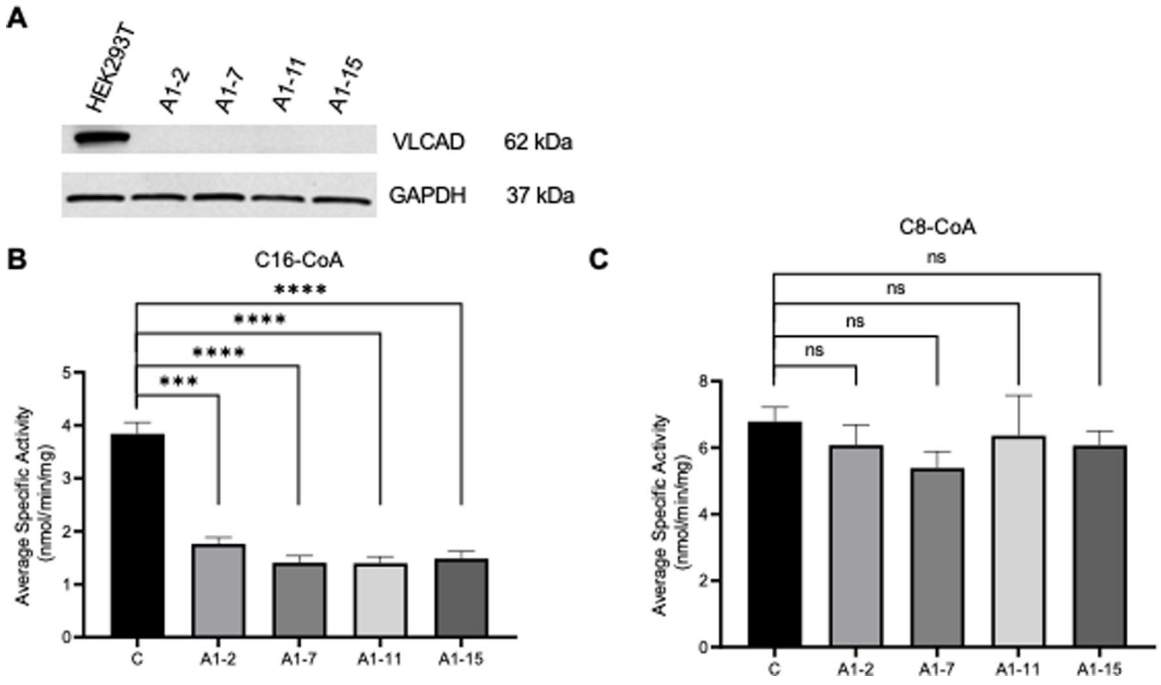

Figure 2: VLCDAD protein and enzyme activity in cellular extracts from control and *ACADVL* null HEK293T lines.

(A) Western blot for VLCAD confirms its absence in clonal lines A1–2, A1–7, A1–11, and A1–15. Molecular mass markers are from Precision Plus Protein Dual Color Standards (BioRad)mix. (B, C) Enzymatic activity of HEK293 *ACADVL* KO extracts measure with palmitoyl-CoA (B) and octanoyl-CoA as substrate (C). All assays were performed in triplicates. Means and standard deviations calculated with an unpaired t-test are shown. ****p<0.0001, ***p<0.001, ns = no statistical difference.

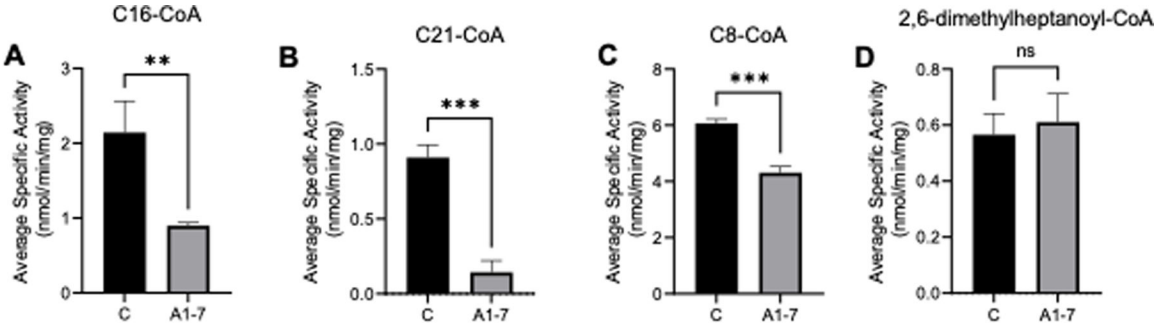

Figure 3: ACAD enzymatic activity of control and *ACADVL* HEK293T ACADVL null clone A1–7.

Activity of control and clone A1–7 were measured with palmitoyl-CoA (A), VLCAD (heneicosanoyl-CoA (C21)) (B), octanoyl-CoA (C), and 2,6-dimethylheptanoyl-CoA (D) as substrates. Assays were performed in triplicates. Means and standard deviations were calculated using an unpaired t-test. ***p<0.001, **p<0.01, ns = no statistical difference.

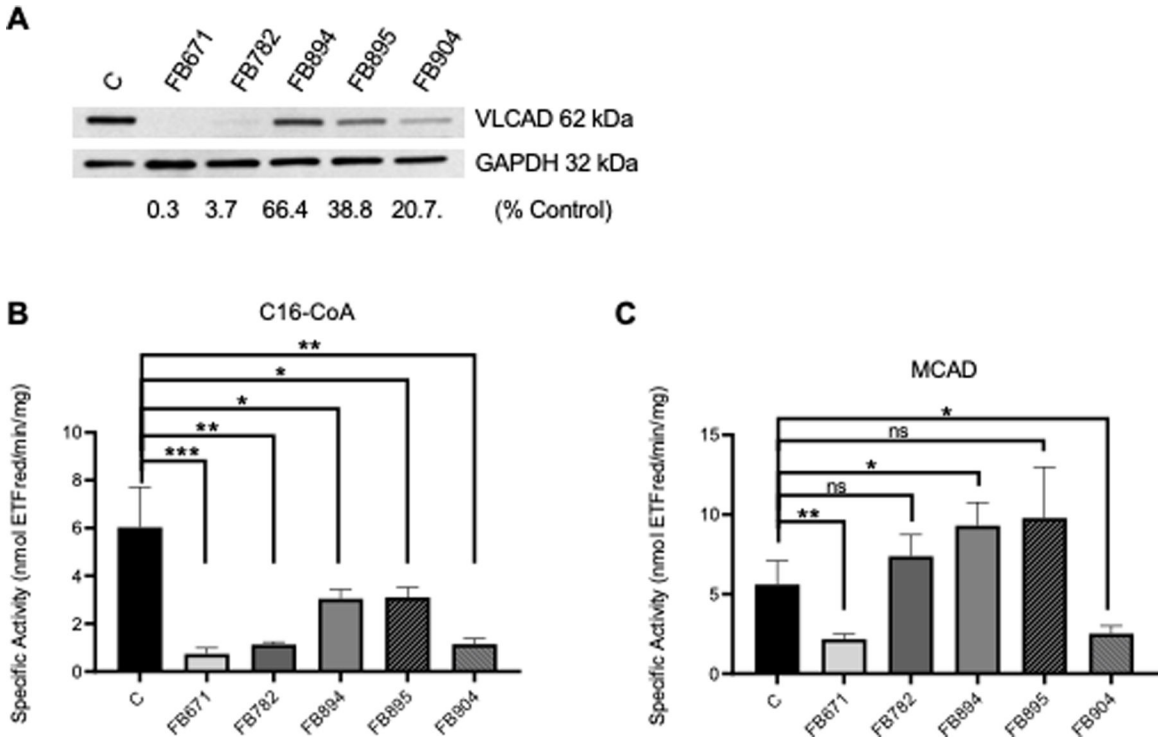

Figure 4: Western blotting and enzymatic activity of VLCAD deficient patient-derived fibroblasts.

Western blot of VLCAD deficient patient and control fibroblasts for detection of VLCAD and GAPDH (A). Enzymatic assay using palmitoyl-CoA or (B), octanoyl-CoA as substrate (C). Activity assays were performed in triplicate. Means and standard deviations were calculated using an unpaired t-test. ***p<0.001, ns = no statistical difference.

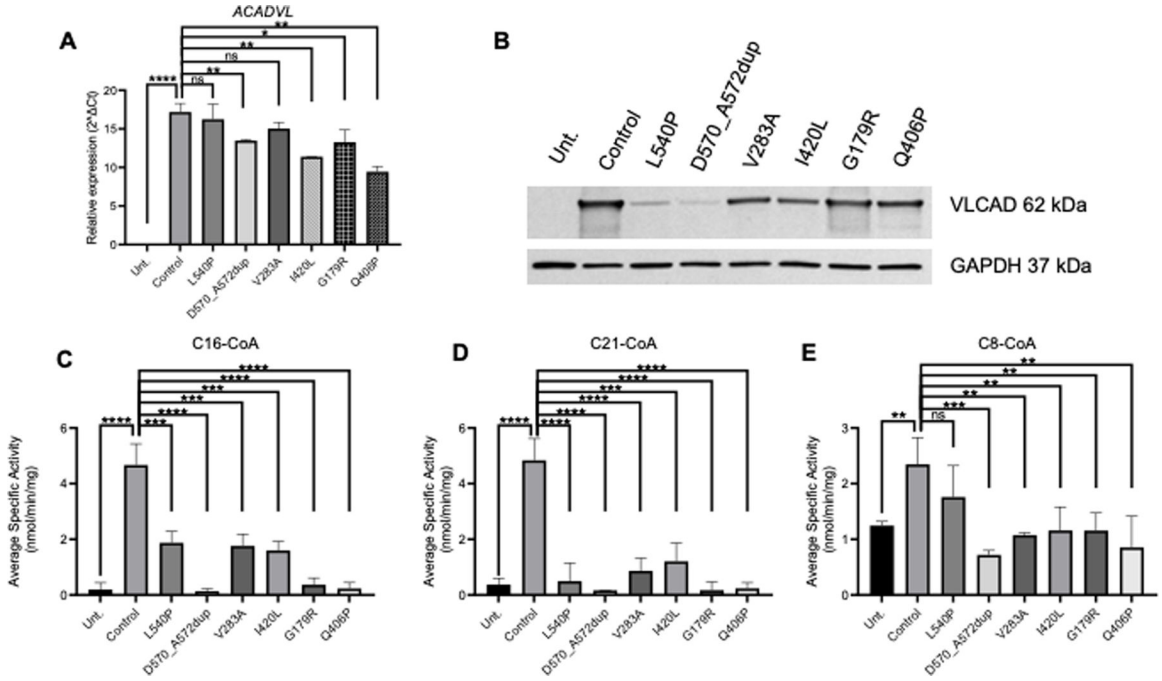

Figure 5: Expression of ACADVL VUS inserts in a *ACADVL* null HEK293T cell line.

Quantitative PCR of *ACADVL* mRNA from HEK293T untransfected, or transfect with wild type or variant VLCAD plasmids. Lanes are identified by the amino acid change in the *ACADVL* expression insert. Utr = untransfected (A). Stable VLCAD protein was detected by western blot with GAPDH used as an internal loading standard. Molecular mass standards were Precision Plus Protein Dual Color Standards (BioRad) (B). Activity assay of cellular extracts following transfection with palmitoyl-CoA (C), heneicosanoyl-CoA (C21) (D), and octanoyl-CoA (E) as substrate. Assays were performed in triplicates. Means and standard deviations were using an unpaired t-test showing significant difference, ****p< 0.0001, ns = no statistical difference.

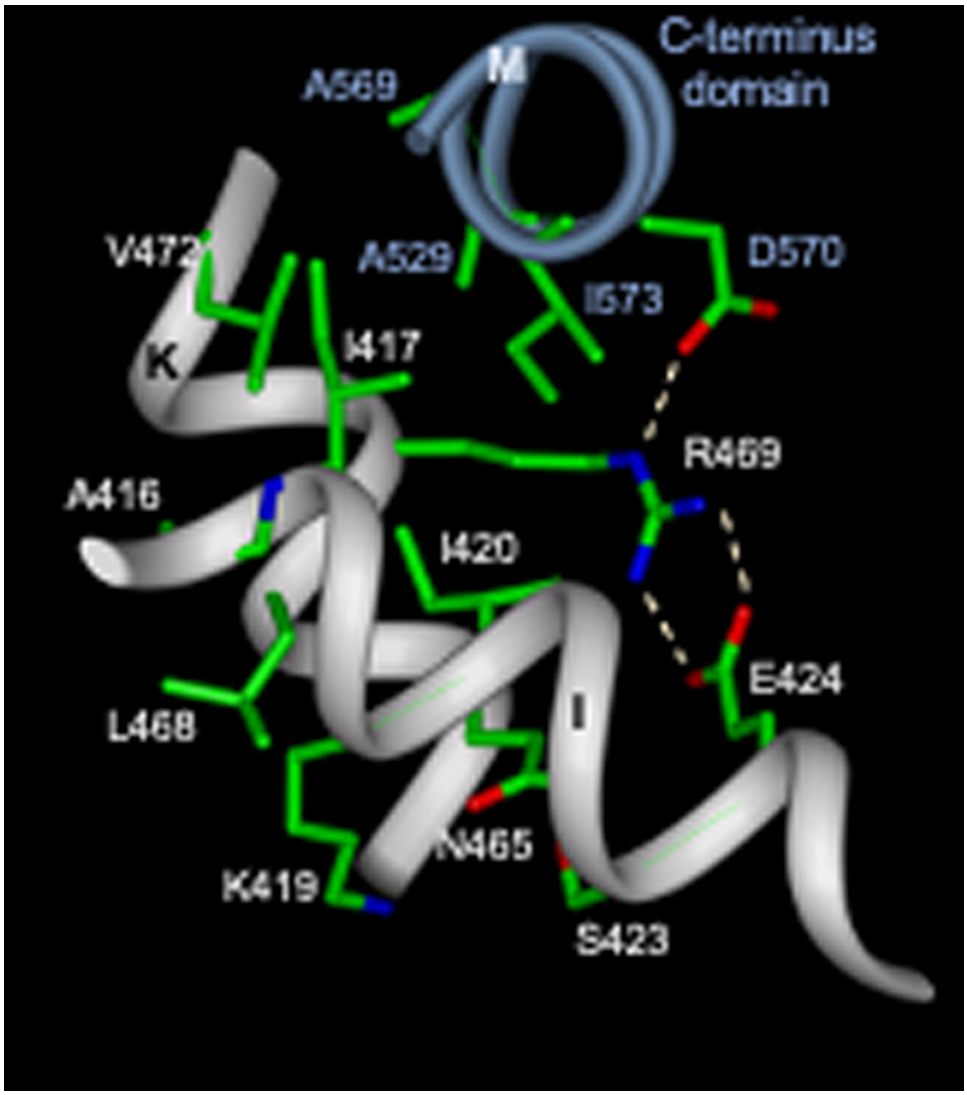

Figure 6: Ribbon representation of relevant area of VLCAD depicting the location of Ile420, interacting residues, and juxtaposed residues that could be affected indirectly by its replacement.

An Ile420 (380 mature numbering) to Leu would affect alignment of Arg469 guanidinium nitrogen to interact with E424 and D570. The published atomic coordinates for VLCAD, 3B96.pdb, was used for the modeling [23].

Table 1.

Identified ACADVL mutations and their corresponding pcDNA3.1(+) plasmid designations and corresponding fibroblast line origin.

Cell Line Origin	Mutation	Plasmid ID	Experimental Findings	Current ClinVar Status	Proposed ClinVar Status
FB826	Control	ACADVL-C	VLCAD protein: normal Enzyme activity: normal	--	--
FB671	c.1619T>C, p.Leu540Pro	ACADVL-1619	VLCAD protein: reduced Enzyme activity: reduced	VUS (not reported)	Pathogenic
FB671	c.1707_1715dup, p.Asp570_Ala572dup	ACADVL-1707	VLCAD protein: reduced Enzyme activity: reduced	VUS	Pathogenic
FB782	c.848T>C, p.Val283Ala	ACADVL-848	VLCAD protein: reduced Enzyme activity: reduced	Pathogenic	Pathogenic
FB782	c.1248A>C, p.Ile420Leu	ACADVL-1248	VLCAD protein: reduced Enzyme activity: reduced	VUS (not reported)	Pathogenic
FB894, FB895	c.535G>A, p.Gly179Arg	ACADVL-535	VLCAD protein: normal Enzyme activity: reduced	VUS	Pathogenic
FB904	c.1217A>C, p.Gln406Pro	ACADVL-1217	VLCAD protein: normal Enzyme activity: reduced	VUS	Pathogenic